Numerical Heat Transfer, Part A: Applications: An International Journal of Computation and Methodology
Publication details, including instructions for authors and subscription information:
http://www.tandfonline.com/loi/unht20

CFD Simulation of Boiling Flows Using the Volume-of-Fluid Method within OpenFOAM

Christian Kunkelmann [a] & Peter Stephan [a]
[a] Institute of Technical Thermodynamics, Technische Universität Darmstadt, Darmstadt, Germany
Version of record first published: 07 Dec 2009.

To cite this article: Christian Kunkelmann & Peter Stephan (2009): CFD Simulation of Boiling Flows Using the Volume-of-Fluid Method within OpenFOAM, Numerical Heat Transfer, Part A: Applications: An International Journal of Computation and Methodology, 56:8, 631-646

To link to this article: http://dx.doi.org/10.1080/10407780903423908

Numerical Heat Transfer, Part A, 56: 631–646, 2009

ISSN: 1040-7782 print/1521-0634 online
DOI: 10.1080/10407780903423908

Taylor & Francis
Taylor & Francis Group

CFD SIMULATION OF BOILING FLOWS USING THE VOLUME-OF-FLUID METHOD WITHIN OPENFOAM

Christian Kunkelmann and Peter Stephan
Institute of Technical Thermodynamics, Technische Universität Darmstadt, Darmstadt, Germany

This article describes the implementation and validation of a nucleate boiling model in the volume-of-fluid solver of OpenFOAM. Emphasis is put on the implementation of the contact line evaporation, which can typically not be resolved by the numerical grid, and on the conjugate heat transfer between solid and fluid. For validation, the sucking interface problem and the growth of a spherical bubble have been simulated successfully. In order to validate the contact line model and the conjugate heat transfer, the growth of a bubble from a heated steel foil has been calculated.

INTRODUCTION

Boiling is one of the most efficient ways to achieve high heat fluxes at a reasonable wall superheat. In order to allow smaller safety margins for industrial applications, there is a need to accurately predict both the heat transfer coefficient and the critical heat flux at which the wall superheat increases dramatically. However, many of the physical phenomena that occur in boiling and their interaction are still not well understood. Consequently, nonempirical predictive tools are rare.

An accurate prediction tool for nucleate boiling in the isolated bubble regime has been developed by Fuchs et al. [1]. The model uses a Langrangian mesh that follows the motion of the liquid–vapor interface. The major drawbacks of this approach are the assumption that the bubble is spherical until it detaches from the heating wall, and the fact that the model cannot be used to simulate the interaction between multiple bubbles. Very robust methods like volume-of-fluid (VOF) and level-set have been developed, which can capture a moving interface on a fixed grid. Unfortunately, the modeling of phase change is more complex in such an approach because the position of the liquid–vapor interface does not coincide with a boundary of the computational domain. Son et al. [2] combined a level-set-method

Received 24 July 2009; accepted 17 September 2009.

This paper was presented at the 7th International Conference on Boiling Heat Transfer in Florianópolis, Brasil 2009.

The authors would like to thank Steffen Hardt for the support and numerous fruitful discussions, and the German Research Foundation (DFG) for the project support.

Address correspondence to Peter Stephan, Institute of Technical Thermodynamics, Technische Universität Darmstadt, Petersenstraße 30, 64287 Darmstadt, Germany. E-mail: pstephan@ttd.tu-darmstadt.de

NOMENCLATURE

A	dispersion constant, J	δ	film thickness, m
b_{cl}	thickness of contact line region, m	δ'	gradient of film thickness, –
c_p	specific heat capacity, J/(kg K)	η	coordinate orthogonal to wall, m
F	volume fraction, –	ϑ	wetting angle, –
$\vec{f}$	momentum source term, N/m^3	λ	thermal conductivity, W/(m K)
$\dot{h}$	enthalpy source term, W/m^3	μ	dynamic viscosity, Pa · s
h_{lv}	specific heat of vaporization, J/kg	ξ	coordinate parallel to wall, m
j_{ev}	evaporating mass flux, kg/(m^2 s)	ρ	density, kg/m^3
$\dot{m}_{ev}$	evaporation rate, kg/s	σ	surface tension, N/m
p	pressure, Pa		
$\dot{q}$	heat flux, W/m^2	**Subscripts**	
$\dot{Q}$	heat flow, W	c	capillary
$\tilde{Q}^*$	heat flow per unit contact line length, W/m	cl	contact line
		g	gravity
r	radial coordinate, m	int	interface
R	bubble radius, m	l	liquid
R_{gas}	gas constant, J/(kg K)	mic	micro region
R_{int}	interfacial heat resistance, (K m^2)/W	ref	reference
t	times, s	sat	saturation
T	temperature, K	ST	surface tension
$\vec{u}$	velocity vector, m/s	v	vapor
α	evaporation coefficient, –	w	wall

with a phase change model and achieved good predictions for the growth of a single vapor bubble on a heated wall. The evaporating mass flux is calculated by evaluating the local temperature gradients at the interface and by assuming that the interface is at saturation temperature. The contact line evaporation is captured by a microlayer model. The transient heat conduction inside the solid wall is not taken into account. Wu et al. [3] coupled this phase change model to a moving mesh method and simulated subcooled nucleate boiling; while Li and Dhir [4] extended the model in order to simulate the growth of bubbles in a shear flow and on an inclined heater surface. The bubble shape predicted by the model was compared to experimental data and good agreement was found. Another approach to model phase change with an interface capturing method was presented by Welch and Wilson [5]. A VOF method is used to simulate the interface dynamics, while the thermal boundary condition at the liquid–vapor interface is similar to the one used in references [2–4]. The model was successfully used to simulate 1-dimensional phase change problems and film boiling. Welch and Rachidi [6] extended the model and applied it to compute film boiling with conjugate heat transfer. Very recently, Hardt and Wondra [7] have presented a different thermal boundary condition for the liquid–vapor interface. The evaporating mass flux is calculated based upon the superheat at the interface and the interfacial resistance. The evaporation is implemented by liquid side mass sinks and vapor side mass sources. Several 1-dimensional phase change problems, as well as film boiling and droplet evaporation, were successfully simulated. The contact line evaporation, which is of special interest for nucleate boiling, is not taken into account. One approach to couple the microscopic phenomena in the contact line region to a macroscopic calculation has been developed by Stephan and Busse [8].

Their model was developed and used to calculate the evaporation of stationary menisci on grooved heat pipe evaporators. Micro and macro regions are simulated and coupled iteratively.

The aim of the present work was to implement the phase change model of Hardt and Wondra [7] into the open source CFD package OpenFOAM, which is based upon the work of Weller et al. [9]. The implementation was validated with several test cases. Furthermore, the solver was extended by a model for the near contact line region, which is based upon the approach developed by Stephan and Busse [8].

NUMERICAL METHOD

Governing Equations

In this section, the underlying equations for mass, momentum, energy, and volume fraction are defined. Liquid and vapor are both treated as incompressible, Newtonian fluids. The mass conservation equation is given as

$$\nabla \cdot (\rho \vec{u}) = \dot{\rho} \tag{1}$$

The source term on the right hand side of Eq. (1) accounts for the phase change and will be explained below. It is important to note that the mass is globally conserved in spite of the local source terms. All of the mass that is removed on the liquid side of the interface reappears on the vapor side. The momentum balance equation can be written as

$$\frac{\partial \rho \vec{u}}{\partial t} + \nabla \cdot (\vec{u} \cdot \rho \vec{u}) = -\nabla p + \nabla \cdot (\mu \nabla \vec{u}) + \vec{f}_{\mathrm{ST}} + \vec{f}_g \tag{2}$$

The momentum source terms $\vec{f}_{\mathrm{ST}}$ and $\vec{f}_g$ in Eq. (2) represent surface tension and gravity, respectively. The surface tension term is modeled according to the approach of Brackbill et al. [10]. No additional source term is needed to account for the phase change in the momentum balance equation. The vapor recoil force is captured by the convective term of Eq. (2). The energy balance is given by

$$\frac{\partial \rho c_p T}{\partial t} + \nabla \cdot (\vec{u} \cdot \rho c_p T) = \nabla \cdot (\lambda \nabla T) + \dot{h} \tag{3}$$

The source term on the right hand side of Eq. (3) represents the heat that is removed by evaporation. The volume fraction field is transported in a purely convective manner.

$$\frac{\partial F}{\partial t} + \nabla \cdot (\vec{u} F) = \frac{\dot{\rho}}{\rho} F \tag{4}$$

The source term on the right hand side of Eq. (4) is necessary because, due to the local mass source terms, the velocity field is not divergence free. The VOF method that is implemented in OpenFOAM does not solve Eq. (4) implicitly, but using a multidimensional universal limiter with explicit solution (MULES) algorithm. Together with an interface compression algorithm, this method ensures a sharp

interface and limits the volume fraction field to values between 0 and 1. The material properties in Eqs. (1)–(4) are determined as a function of the volume fraction.

$$\gamma = F \cdot \gamma_l + (1 - F) \cdot \gamma_v \tag{5}$$

Herein, γ is a variable for any of the material properties.

Phase Change Model

The phase change is modeled according to the work of Hardt and Wondra [7]. The model will be described very briefly in this section. The evaporating mass flux at the liquid–vapor interface is calculated as

$$j_{\text{ev}} = \frac{T_{\text{int}} - T_{\text{sat}}}{R_{\text{int}} h_{lv}} \tag{6}$$

Herein, R_{int} is the heat resistance of the liquid–vapor interface. Based on the considerations of Schrage [11], this variable can be expressed by

$$R_{\text{int}} = \frac{2 - \alpha}{2\alpha} \frac{\sqrt{2\pi R_{\text{gas}}}}{h_{lv}^2} \frac{T_{\text{sat}}^{3/2}}{\rho_v} \tag{7}$$

The amount of liquid that evaporates is calculated locally. The resulting source term field is smeared over a few cells. The evaporating mass is taken away on the liquid side of the interface and reappears on the vapor side. Details on the procedure are given by Hardt and Wondra [7].

It is important to note that Eqs. (6) and (7) are derived from considerations on length scales which are several orders smaller than the typical grid size used for the simulations in this work. Nevertheless, the model leads to the correct evaporation rate because it acts like a control loop. The more the temperature at the interface deviates from the saturation temperature, the more liquid evaporates and the more the temperature drops locally. This ensures that the temperature at the liquid–vapor interface always stays very close to (little above) the saturation temperature. The difference is very small compared to the macroscopic temperature differences, and its influence on the macroscopic heat transport by conduction and convection is negligible. The result is comparable to an approach in which the saturation temperature at the liquid–vapor interface is fixed in order to calculate the local evaporation rate (as in [2–6]). However, the continuum-field formulation of this phase change model makes it more straightforward to implement.

Contact Line Evaporation

Microlayer evaporation. This section is dedicated to the implementation of a model which captures the physical phenomena near the contact line. One of the main problems is the fact that the interface in a VOF method is smeared over at least one grid cell. In the simulations of this work, the interface was typically smeared over

two to three cells. Therefore, the contact line is not a real line, but rather an area or a sum of discrete grid faces where the gradient of the volume fraction is non zero.

Stephan and Busse [8] derived a fourth order, ordinary differential equation for the film thickness evolution in the so called micro region. The micro region is defined as the region in which the adhesion forces between fluid molecules and wall molecules, and the effect of curvature on the local thermodynamic equilibrium are important. In a microscopic scale, there is no contact line, as can be seen in Figure 1. For $\xi < 0$, there is an adsorbed layer of molecules on the solid wall. No liquid evaporates in this region. At $\xi = 0$, the curvature suddenly increases and the thickness of the liquid film starts to grow. As the distance between the liquid–vapor interface and the wall becomes larger, the adhesion forces decrease rapidly and the meniscus shape is governed by macroscopic hydrodynamics. The evolution of film thickness and slope, capillary pressure, and heat flux can be obtained by solving a system of first order differential equations that is derived from the abovementioned fourth order differential equation.

$$\frac{\mathrm{d}\delta}{\mathrm{d}\xi} = \delta' \tag{8}$$

$$\frac{\mathrm{d}\delta'}{\mathrm{d}\xi} = \frac{(1+\delta'^2)^{3/2}}{\sigma}\left(p_c - \frac{A}{\delta^3}\right) \tag{9}$$

$$\frac{\mathrm{d}p_c}{\mathrm{d}\xi} = -\frac{3\mu_l \dot{Q}^*}{\rho_l h_{\mathrm{lv}} \delta^3} \tag{10}$$

$$\frac{\mathrm{d}\dot{Q}^*}{\mathrm{d}\xi} = \frac{T_{\mathrm{wall}} - T_{\mathrm{sat}}(1 + p_c/(\rho_l h_{\mathrm{lv}}))}{\delta/\lambda_l + R_{\mathrm{int}}} \tag{11}$$

The solution of Eqs. (8)–(11) is the development of the film thickness, the curvature, the capillary pressure, and the heat flux in the micro region for a given wall superheat. An example is shown in Figure 2. The heat flux reaches its maximum

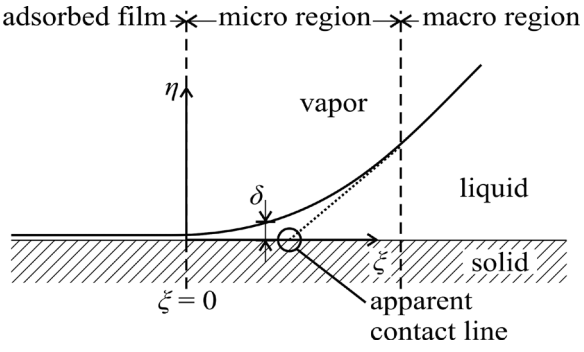

Figure 1. Definition of the micro region and the apparent contact line.

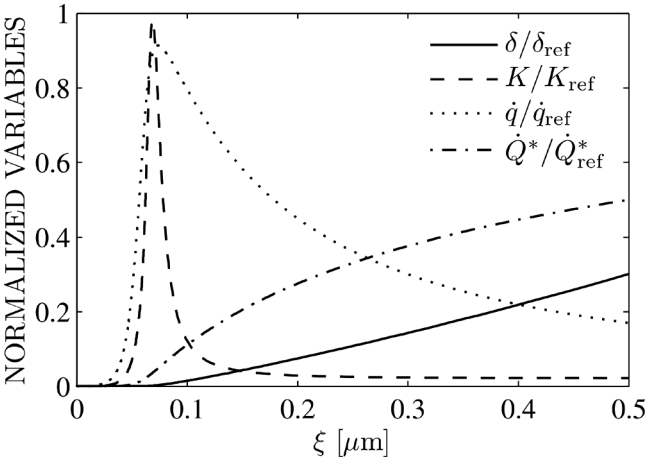

Figure 2. Evolution of normalized film thickness, curvature and heat flux in the micro region. Results obtained for water at 1013 mbar and a wall superheat of 5 K ($\delta_{ref} = 0.5\,\mu m$, $K_{ref} = 1.2 \cdot 10^7 \cdot 1/m$, $\dot{q}_{ref} = 1.1 \cdot 10^8\,W/m^2$, and $\dot{Q}^*_{ref} = 40\,W/m$).

value approximately at the same point where the curvature becomes maximal. However, the heat flux does not drop as rapidly as the curvature, because the liquid film is still very thin and has a low heat resistance.

Coupling of macro and micro region. The most important value needed for coupling the contact line model to a CFD simulation is the integrated heat flux.

$$\dot{Q}^*_{mic} = \int_{\xi=0}^{\xi_{mic}} \dot{q}(\bar{\xi}) d\bar{\xi} \tag{12}$$

This value gives the amount of heat per unit contact line length which is transferred in the micro region. The value of ξ_{mic} in Eq. (12) describes the width of the micro region. It has to be chosen under the condition that the adhesion forces and the effect of the curvature on the thermal equilibrium are negligible for any $\xi > \xi_{mic}$.

As the solution procedure for solving Eqs. (8)–(11) is quite time consuming, the results were correlated to the wall superheat and the material properties prior to the simulation. Hence, the system of differential equations does not need to be solved in each time step. For a given set of material properties, the solution depends only on the wall superheat at the contact line. The correlation

$$\dot{Q}^*_{mic} = \sum_{n=1}^{N} a_n^{(Q)} (\Delta T)^{1/n} \tag{13}$$

was found to match the data in a very accurate way. The heat flow in the micro region as a function of wall superheat for different fluids is shown in Figure 3. The values obtained for water are approximately one order of magnitude higher than

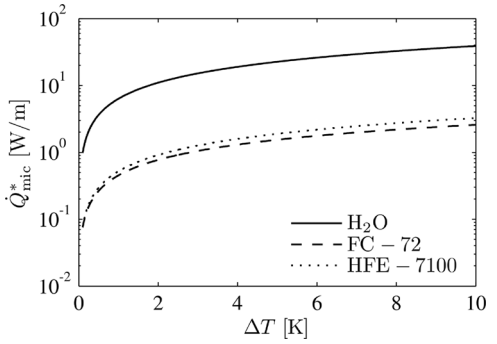

Figure 3. Integrated heat flux in the micro region over wall superheat for water and FC-72 at 1013 mbar and HFE-7100 at 500 mbar.

those obtained for the refrigerants FC-72 and HFE-7100. This difference can be explained by the higher thermal conductivity of water.

As the thickness of the contact line b_{cl} in a VOF method is of the order of some grid sizes and therefore larger than ξ_{mic} (see Figure 4), a spatial gap is generated between the largest length scale of sub-grid contact line model and the smallest length scale of the CFD simulation. To correct this, a transition region between those two length scales is defined. In this region, the adhesion forces and the effect of the curvature on the thermal equilibrium are negligible. Furthermore, the liquid–vapor interface has almost a constant slope for $\xi_{\mathrm{mic}} < \xi < b_{\mathrm{cl}}$. Thus, Eqs. (8)–(11) can be simplified and solved analytically. The result is the integrated heat flux in the transition region.

$$\dot{Q}^*_{\mathrm{trans}} = \frac{\lambda_l (T_w - T_{\mathrm{sat}})}{\tan \vartheta} \ln\left(1 + \frac{(b_{\mathrm{cl}} - \xi_{\mathrm{mic}}) \cdot \tan \vartheta}{\delta_{\mathrm{mic}} + \lambda_l R_{\mathrm{int}}}\right) \tag{14}$$

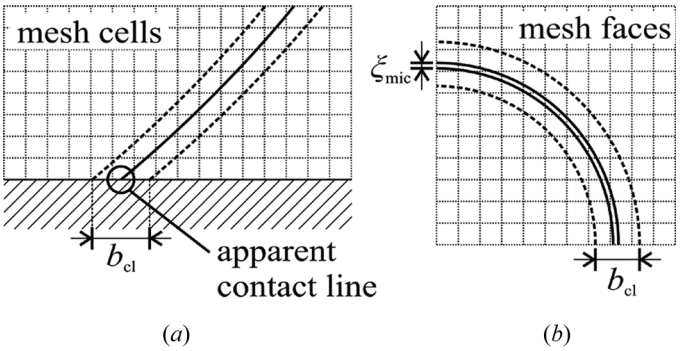

Figure 4. Comparison of the physical contact line region and its representation in a VOF approach. (*a*) Side view and (*b*) top view.

Herein, δ_{mic} is the film thickness at ξ_{mic}. A similar correlation to Eq. (13) has been determined for this variable. The total heat transferred in the near contact line region of the VOF method with a thickness of b_{cl} is given by

$$\dot{Q}_{cl} = (\dot{Q}^*_{mic} + \dot{Q}^*_{trans}) \cdot l_{cl} \tag{15}$$

The near contact line region in the CFD simulation is not adiabatic. Therefore, the macroscopic CFD simulation already resolves some of the heat transfer in this region and only the difference,

$$\Delta\dot{Q}_{cl} = \dot{Q}_{cl} - \dot{Q}^{(CFD)}_{cl} \tag{16}$$

must be imposed as an additional heat flux that is removed from the wall and intensifies the evaporation locally. The coupling between the contact line model and the macroscopic CFD calculation is done via two variables: The local wall superheat $\Delta T = T_w - T_{sat}$ and the heat transferred in the near contact line region $\dot{Q}_{cl}$. The local wall superheat is the input parameter for the micro region model and can be taken from the CFD simulation. The heat transfer in the near contact line region is a boundary condition for the CFD simulation and can be taken from the micro region model. Both variables are exchanged iteratively until convergence is reached.

RESULTS AND DISCUSSION

Sucking Interface Problem

The sucking interface problem is used as a 1-dimensional test case for the phase change model and its implementation in the VOF solver of OpenFOAM. It can be described as follows. Superheated liquid is separated from an adiabatic wall by a vapor film. The coordinate x refers to the direction perpendicular to the wall. Heat is transferred by conduction from the superheated liquid to the liquid–vapor interface where it leads to evaporation. The liquid–vapor interface and the bulk vapor are assumed to be at saturation temperature. Due to the 1-dimensional geometry of the problem and the abovementioned assumptions, the problem can be solved analytically by using a similarity solution. Details about the problem and its analytical solution are given by Welch and Wilson [5]. The initial condition of the simulation is a defined temperature profile which is taken from the similarity solution at 0.1 s. The temperature drops from the superheated level to saturation temperature within a length of less than 0.5 mm. The development of the interface position as a function of time is shown in Figure 5. The model predicts the development very well. Due to the lower density of the vapor, the liquid is pushed away from the wall as it evaporates. In the same time, due to heat diffusion, the thickness of the thermal layer increases which leads to a decreasing evaporation rate. The initial temperature profile and simulation results at 1.1 s are shown in Figure 6. The results agree very well with the analytical solution. This test case is of special interest for this study because the phase change model does not fix the temperature at the liquid–vapor interface to the saturation temperature explicitly. Nevertheless, the temperature profiles in Figure 6 show that the temperature at the liquid–vapor interface is very

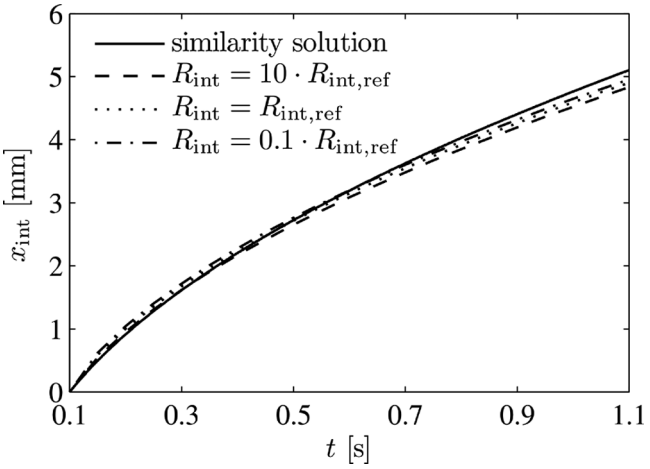

Figure 5. Sucking interface problem. Influence of interfacial resistance and comparison to analytical solution (mesh size: 10 μm, liquid superheat: 5 K).

close to the saturation temperature. The difference is small and does not influence the macroscopic heat transport.

It is important to note that the influence of the interfacial resistance is negligible. The value has been varied in a range of two orders of magnitude. The reference value corresponds to the result of Eq. (7) with an evaporation coefficient of $\alpha = 1$. The results which are shown in Figures 5 and 6, prove that the simulation results are not sensible to this variation of two orders of magnitude. This behavior was expected because the interfacial resistance is much smaller than the resistance of

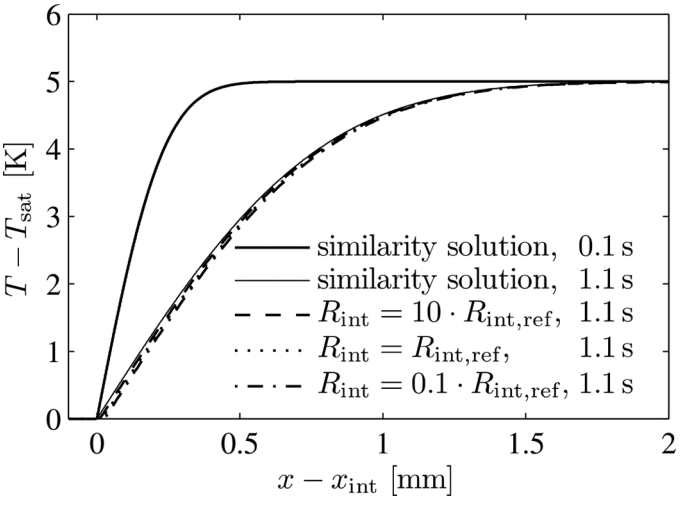

Figure 6. Sucking interface problem. Temperature profiles at 0.1 s (initial condition) and 1.1 s (analytical and numerical results).

the liquid region that contains the thermal layer. In nucleate boiling simulations, the interfacial resistance will be nonnegligible only in the near contact line region. This region, however, is treated by the contact line model and not by the macroscopic CFD simulation.

Growth of a Spherical Bubble in a Superheated Liquid

The second test case for the phase change model was the growth of a spherical bubble in an infinitely extended superheated liquid. The phenomenon and the different stages of growth are well described by Plesset and Zwick [12]. After an initial stage during which the bubble growth is controlled by surface tension and inertia effects, the growth is controlled only by the rate at which heat can be transferred from the superheated liquid to the liquid–vapor interface. During the second stage, which is the subject of this study, it can be assumed that the bulk vapor and the liquid–vapor interface are at saturation temperature. Scriven [13] has derived an analytical solution for this situation. A similarity solution is used to predict the growth rate of a vapor bubble in a superheated liquid. Similar to the sucking interface problem, the analytical solution permits to calculate an initial condition (i.e., the temperature profile) for the simulations and to validate the numerical results.

The initial temperature profiles for the numerical simulations were taken at an instant when the analytical solution predicted a bubble radius between 0.1 and 0.2 mm. The thickness of the thermal layer shall be defined as

$$\delta_{\text{therm}} = r(T = T_{\text{sat}} + 0.99 \cdot (T_{\infty} - T_{\text{sat}})) - R(t) \tag{17}$$

In Figure 7, this value is plotted as a function of the liquid superheat for bubbles with a radius of 0.1 mm. The values are results of the similarity solution that was presented by Scriven [13]. The values decrease drastically with increasing liquid superheat. In nucleate boiling conditions, the typical liquid superheat very close to the heating wall is significantly above 5 K. In this range, the thickness of the thermal layer is less than 10 μm. In order to simulate the phase change accurately, this characteristic length must be resolved by the grid.

The simulations for the axisymmetric bubble growth were performed on two different grid types: a very fine axisymmetric grid and a coarser 3-dimensional grid with adaptive grid refinement at the liquid–vapor interface. OpenFOAM offers adaptive grid refinement only for 3-dimensional grids. The minimum grid size for both types was 1 μm for water and 0.5 μm for the two refrigerants FC-72 and HFE-7100. No difference was found between the results of the axisymmetric simulations and those of the 3-dimensional simulation with adaptive grid refinement. Consequently, the phase change model can easily be used for 3-dimensional simulations in future.

The development of the bubble radius with time for different fluids at a liquid superheat of 5 K is shown in Figure 8. The results match the analytical solution very well. However, a very fine grid is required in order to resolve the temperature profile at the liquid–vapor interface. It is interesting to note that the grid for the simulations with water is twice as coarse as it is for the simulations with the refrigerants. Although, the thermal layer has approximately the same or even lower thickness for the refrigerants, as can be seen in Figure 7. It seems that the higher thermal

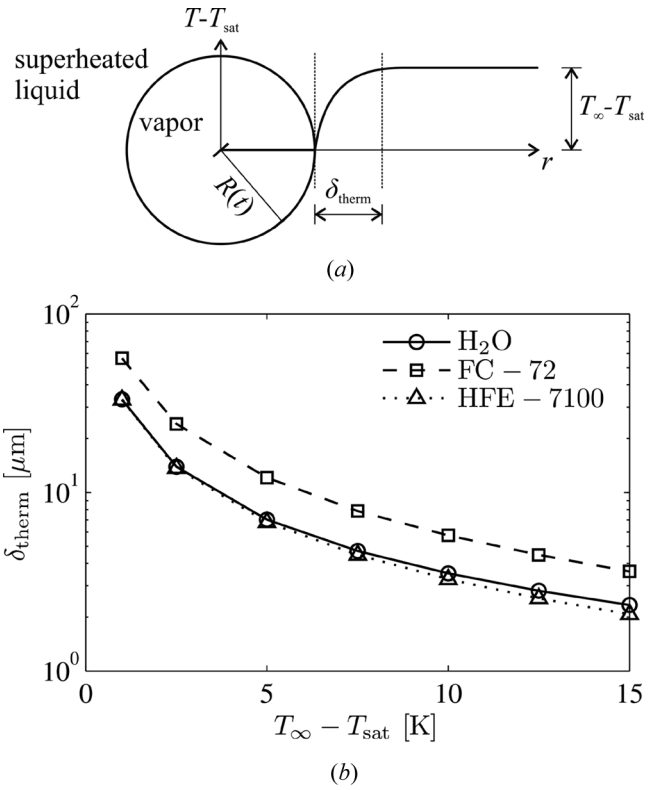

Figure 7. Spherical bubble growth. (*a*) Geometry of the problem and (*b*) thickness of thermal layer over liquid superheat for water and FC-72 at 1013 mbar and HFE-7100 at 500 mbar.

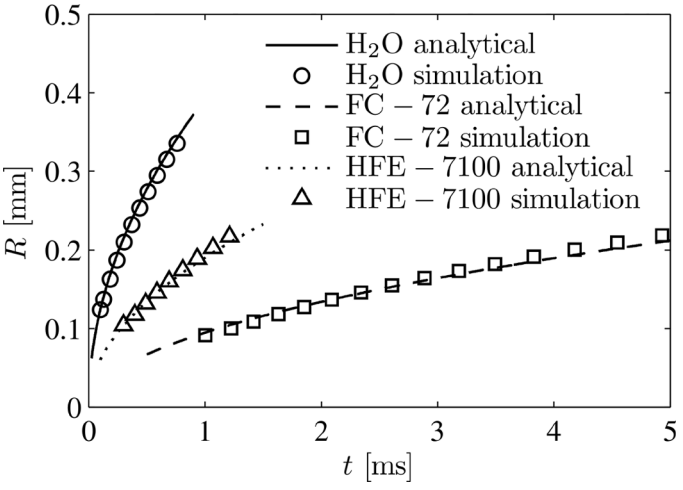

Figure 8. Spherical bubble growth. Bubble radius over time for water and FC-72 at 1013 mbar and HFE-7100 at 500 mbar (liquid superheat: 5 K).

conductivity of water compared to the refrigerants is favorable for the phase change modeling. Due to the discreteness of the grid, the initialization of the interface position via the volume fraction leads to small errors. The interface position cannot be initialized accurately, but only with an uncertainty around the cell size. Consequently, the thermal layer might initially be a little misplaced with respect to the interface. The higher the thermal conductivity, the faster the thermal layer can rearrange slightly in order to fit to the interface position.

Growth and Detachment of a Bubble from a Heated Wall

In this section, some preliminary simulation results for nucleate boiling will be presented. Refrigerant HFE-7100 is boiled at a pressure of 500 mbar on a steel heating foil with a thickness of 50 μm. In contrast to the preceding sections, no analytical solution can be used to validate the numerical results. Therefore, the material, the geometry, and the conditions have been chosen according to the high resolution experiments presented by Wagner et al. [14]. In this experimental work, the steel foil is heated by electric current. An artificial nucleation site on the foil ensures that the bubbles grow and detach in the field of view. The results give a very detailed insight into the phenomena at the contact line and the transient heat conduction in the solid wall. The authors measured the temperature imprint of the bubble foot on the back side of the heating foil and used a transient heat conduction model to calculate the local heat flux. Additionally, the temperatures of liquid and vapor were measured with a micro thermocouple which is placed above the heater. The wall temperature is around 15 K above the saturation temperature. In order to accurately compare numerical and experimental data, multiple bubble cycles would have to be simulated until a periodic regime is reached. In a first step, the simulations in this study were performed only for a single bubble event and with a lower wall superheat in order to reduce computation time. Consequently, a quantitative comparison between numerical and experimental results remains a task for future studies.

The numerical simulations are carried out with a wall superheat of 5 K. Initially, the heating foil is isothermal. A small vapor bubble with a radius of 0.05 mm is placed onto its surface. The liquid in vicinity of the wall is superheated. The thermal layer is assumed to be linear with a thickness of 1 mm. This choice is arbitrary as the real thermal layer can only be obtained by simulating multiple bubble cycles. The geometry of the computational domain and the initial thermal layer are illustrated in Figure 9. The entire vapor phase is at saturation temperature at the beginning of the computation. The steel foil is heated by a volumetric heat source while its backside is adiabatic. This corresponds to the electric heating that was used by Wagner et al. [14].

The results of the simulation are shown in Figure 10. During the whole process, the temperature at the liquid–vapor interface is very close to the saturation temperature although this is not explicitly set by the phase change model. As the bubble grows, the isolines of temperature are first moved upwards until the bubble emerges from the superheated liquid layer. When the bubble departs from the heated surface and rises upward, some of the superheated liquid is pulled in its wake. The bubble detaches with a volume of 2.2 mm^3. Wagner et al. [14] observed volumes of around 3.3 mm^3 when the bubbles detached. The difference is probably due to the lower wall

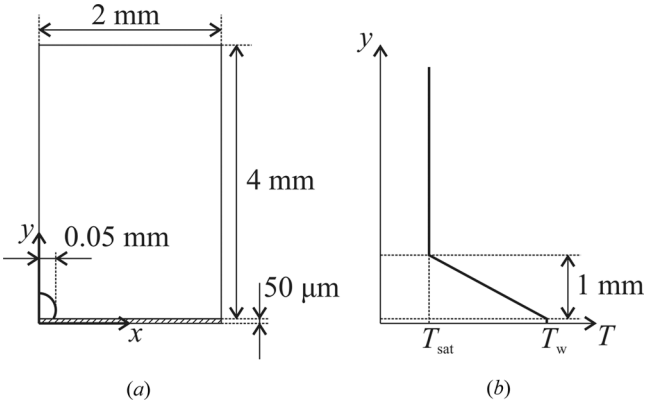

Figure 9. (*a*) Sketch of the computational domain and (*b*) initial thermal layer in the liquid phase and in the solid wall.

superheat imposed in the simulation. The results which are presented by Son and Dhir [2], show that the detachment diameter of bubbles becomes larger with increasing wall superheat.

For better lucidity, the isolines in Figure 10 are shown in the liquid phase only. As the phase change model which is used does not require fixing the vapor temperature to saturation temperature, the energy equation is also solved in the vapor phase. The results are shown in Figure 11. The vapor is clearly superheated in the vicinity of the wall. This can be explained physically by comparing the values of the thermal diffusivity $\lambda/(\rho c_p)$ of vapor and liquid. The thermal diffusivity of the vapor is significantly higher than the thermal diffusivity of the liquid. Therefore, the vapor heats up very quickly. After the bubble detachment, the superheat is more and more diluted as the heat supply by the wall has stopped. The micro thermocouple measurements performed by Wagner et al. [12] also show a significant superheat inside the bubble. However, the authors point out that the results of this measurement were the subjects of strong variations.

The transient heat transport during the entire process is shown in Figure 12. The total heat that is consumed by the evaporation is rising sharply to a maximum. Then, the value decreases until the bubble detaches. After detachment, some

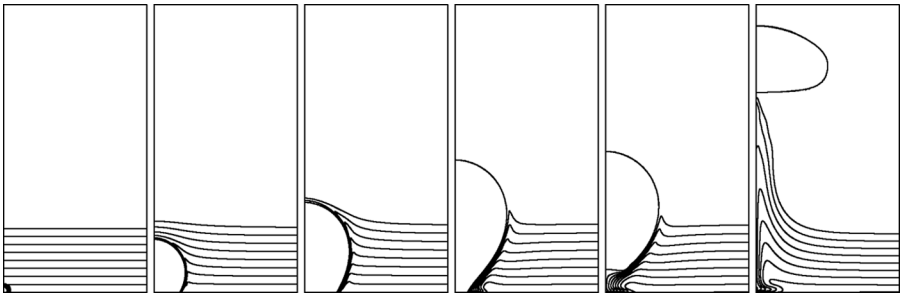

Figure 10. Growth and detachment of a single vapor bubble from a heated surface. Isolines of temperature with $\Delta T = 0.5\,\mathrm{K}$ taken at 0, 5, 13, 24, 26, and 45 ms (from left to right).

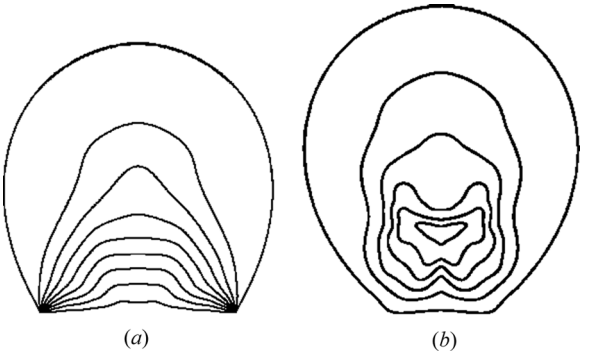

Figure 11. Isolines of temperature with $\Delta T = 0.5$ K in the vapor phase taken at 13 ms (during growth) and 26 ms (after detachment).

evaporation still takes place until the bubble completely emerges from the superheated liquid layer. The other curves in Figure 12, represent the amount of heat that is transferred from the wall to the liquid ($\dot{Q}_l$) and vapor ($\dot{Q}_v$) phase and in the near contact line region ($\dot{Q}_{\mathrm{cl}}$), respectively. Most of the heat that is required for the evaporation is provided by the superheated liquid. During the bubble growth, more heat is removed from the liquid than is supplied from the wall to the liquid. If multiple bubble cycles were simulated, the storage and removal of heat from the liquid layer would become periodic. Although the simulation results show a significant superheat in the vapor phase, the heat transferred to the vapor is negligible compared to the heat which is transferred to the liquid. The heat transferred in the near contact line region is of the same order as the heat transferred into the liquid. As the heat flow in the near contact line region is transferred in a very small area (in this simulation b_{cl} is around 10 μm), it has a strong influence on the transient heat conduction in the wall.

The temperature profiles on the front and back side of the heating foil at different instances are shown in Figure 13. Globally, the wall cools down during

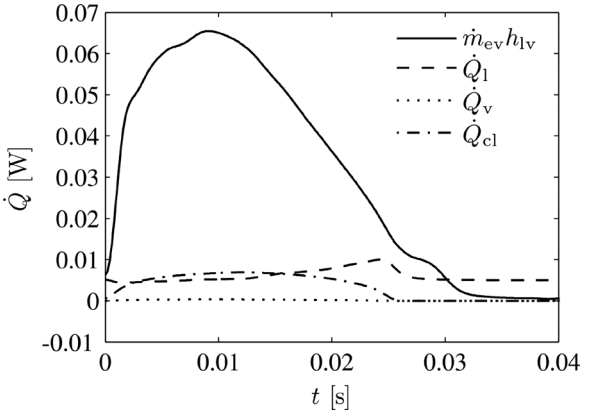

Figure 12. Heat flows during bubble growth and detachment.

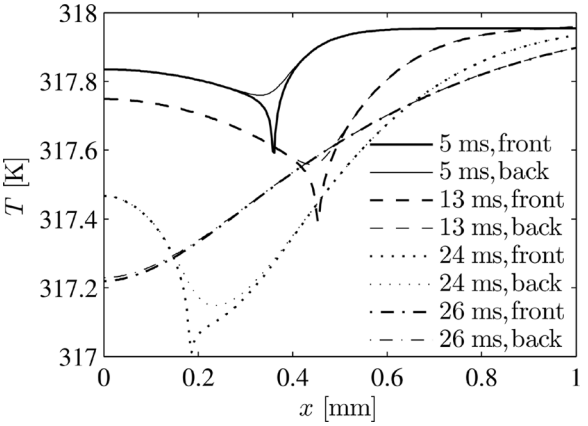

Figure 13. Temperature profiles on front (solid–fluid interface) and back side (adiabatic) of the steel heating foil.

the bubble growth and restarts to heat up when the bubble has departed. At the position of the contact line, the temperature on the front side drops very sharply while the profiles are much smoother on the back side. Although the steel foil is very thin, the temperature difference between the two sides of the heating foil is clearly visible. At 13 ms the contact line is almost stagnating and the minima of the temperature profiles on the front and back side are at the same position. At 24 ms the bubble is about to detach and the contact line is moving quickly. Consequently, the profiles show that the temperature drop on the back side is going behind the one on the front side. After the bubble has detached, the sharp temperature drop vanishes and the temperatures on the two sides are almost identical.

CONCLUSION

The phase change model proposed by Hardt and Wondra [7] has been implemented in the VOF solver of the open source CFD package OpenFOAM. The model and its implementation have been validated with two test cases: the 1-dimensional sucking interface problem and the growth of a spherical vapor bubble in an infinitely extended superheated liquid. The results show good agreement with analytical solutions. The model was extended by a special treatment for the contact line evaporation based on the micro region model of Stephan and Busse [8]. The coupling between the microscopic model and the macroscopic CFD simulation is not trivial as some of the heat that is transferred near the contact line is already captured by the CFD simulation and must not be imposed by the contact line model. The heat flows of the contact line model and the CFD simulation are compared and only the difference is imposed as an additional heat flow, which is removed from the wall and intensifies the evaporation locally. In order to save computation time, the results of the micro region model of Stephan and Busse [8] have been correlated with the wall superheat prior to the simulation. The growth and detachment of a single vapor bubble from a heated steel foil has been simulated. The aim was to test the model for

the near contact line region. A full validation by comparison with experiments could not yet be achieved, as only one bubble cycle with a relatively low wall superheat was simulated. Nevertheless, the preliminary results already give an interesting and detailed insight into the transient heat transport. In particular, the results on the temperature field in the heating wall can help to improve the analysis of experiments where temperature measurements are possible only on the back side of the heater and not directly at the surface, which is in contact with the fluid.

In the future, the model will be used to simulate multiple bubble cycles with higher wall superheats. This will permit to quantitatively compare the simulation results to experimental data. Furthermore, the model will be extended for 3-dimensional simulations in order to simulate bubble coalescence and the growth of bubbles in a shear flow.

REFERENCES

1. T. Fuchs, J. Kern, and P. Stephan, A Transient Nucleate Boiling Model Including Microscale Effects and Wall Heat Transfer, *J. Heat Transfer*, vol. 128, pp. 1257–1265, 2006.
2. G. Son, V. K. Dhir, and N. Ramanujapu, Dynamics and Heat Transfer Associated with a Single Bubble during Nucleate Boiling on a Horizontal Surface, *J. Heat Transfer*, vol. 121, pp. 623–631, 1999.
3. J. Wu, V. K. Dhir, and J. Qian, Numerical Simulation of Subcooled Nucleate Boiling by Coupling Level-Set Method with Moving-Mesh Method, *Numer. Heat Transfer B*, vol. 51, pp. 535–563, 2007.
4. D. Li and V. K. Dhir, Numerical Study of Single Bubble Dynamics during Flow Boiling, *J. Heat Transfer*, vol. 129, pp. 864–876, 2007.
5. S. W. J. Welch and J. Wilson, A Volume of Fluid Based Method for Fluid Flows with Phase Change, *J. Computational Physics*, vol. 160, pp. 662–682, 2000.
6. S. W. J. Welch and T. Rachidi, Numerical Computation of Film Boiling Including Conjugate Heat Transfer, *Numer. Heat Transfer B*, vol. 42, pp. 35–53, 2002.
7. S. Hardt and F. Wondra, Evaporation Model for Interfacial Flows Based on a Continuum-field Representation of Source Terms, *J. Computational Physics*, vol. 227, pp. 5871–5895, 2008.
8. P. C. Stephan and C. A. Busse, Analysis of the Heat Transfer Coefficient of Grooved Heat Pipe Evaporator Walls, *Int. J. Heat Mass Transfer*, vol. 35, pp. 383–391, 1992.
9. H. G. Weller, G. Tabor, H. Jasak, and C. Fureby, A Tensorial Approach to Computational Continuum Mechanics using Object-Oriented Techniques, *Computers in Physics*, vol. 12, pp. 620–631, 1998.
10. J. U. Brackbill, D. B. Kothe, and C. Zemach, A Continuum Method for Modeling Surface Tension, *J. Computational Physics*, vol. 100, pp. 335–354, 1992.
11. R. W. Schrage, *A Theoretical Study of Interphase Mass Transfer*, pp. 32–43, Columbia University Press, New York, 1953.
12. M. S. Plesset and S. A. Zwick, The Growth of Vapor Bubbles in Superheated Liquids, *J. Applied Physics*, vol. 25, pp. 493–500, 1954.
13. L. E. Scriven, On the Dynamics of Phase Growth, *Chem. Eng. Sci.*, vol. 10, pp. 1–13, 1959.
14. E. Wagner, P. Stephan, O. Koeppen, and H. Auracher, High Resolution Temperature Measurements at Moving Vapor/Liquid and Vapor/Liquid/Solid Interfaces During Bubble Growth in Nucleate Boiling, IBW4 2007, Proc. 4th International Berlin Workshop on Transport Phenomena with Moving Boundaries, Berlin, Germany, pp. 260–277, Technische Universität Berlin, Berlin, Germany, 2007.